Harnessing a Quantum Design Approach for Making Low-Loss Superlenses

Alexey O. Bak,[†] Edward O. Yoxall,[†,‡] Paulo Sarriugarte,[‡] Vincenzo Giannini,[§] Stefan A. Maier,[†] Rainer Hillenbrand,[‡,∥] John B. Pendry,[§] and Chris C. Phillips*[,†]

[†]Experimental Solid State Physics Group, Physics Department, Imperial College, London SW7 2AZ, U.K.
[‡]CIC nanoGUNE Consolider and UPV/EHU, 20018 Donostia-San Sebastián, Spain
[§]Condensed Matter Theory Group, Physics Department, Imperial College, London SW7 2AZ, U.K.
[∥]IKERBASQUE, Basque Foundation for Science, E-48011 Bilbao, Spain

Ⓢ *Supporting Information*

ABSTRACT: Recently, so-called "superlenses", made from metamaterials that are structured on a length scale much less than an optical wavelength, have shown impressive diffraction-beating image resolution, but they use materials with negative dielectric responses, and they absorb much of the light in a way that seriously degrades both the resolution and brightness of the image. Here we demonstrate an alternative "quantum metamaterials" (QM) approach that uses materials structured at the nanoscale, i.e., comparable to an electron wavelength. This allows us to use quantum mechanical design principles to generate structures with a highly elliptical isofrequency dispersion characteristic that circumvents this loss problem. The physics of the loss improvement is analyzed analytically and the QM superlens subdiffraction imaging is modeled numerically, with a finite-element method. Finally, we demonstrate a working QM superlens device, utilizing intersubband transitions between the confined electron states in a III−V semiconductor multiquantum-well. It images down to a resolution of better than ∼λ/10 and has loss figures improved by roughly a decade over previous "classical" designs. This QM approach is an alternative paradigm for designing radiation-manipulating devices and offers the prospect of practical super-resolving devices at new wavelengths and geometries.

KEYWORDS: Metamaterials, superlens, s-SNOM, super-resolution, imaging, hyperlens, quantum well
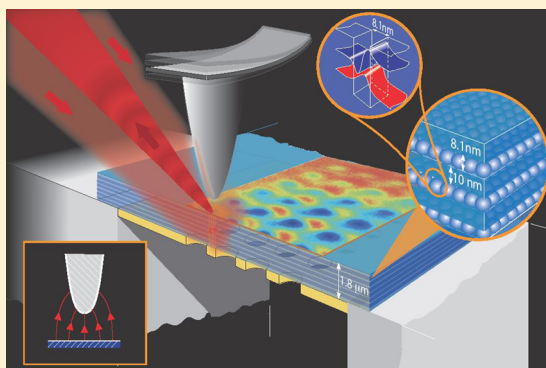
"Classical" metamaterials use subwavelength structuring to generate new optical phenomena, such as negative refraction,[1] cloaking,[2−4] and lenses that collect the near-field components of the light scattered by an object[5−7] so as to image it at a diffraction-beating subwavelength super-resolution (SR). SR has also been demonstrated in "hyperbolic"[8,9] materials, and both approaches have given near-field devices,[5,10−12] and it has been shown that they can subsequently be extended to the far-field with "epsilon-near-zero" (ENZ) materials.[6,13,14] However, these methods all exploit geometrical "effective-medium" structuring with component materials whose dielectric responses are themselves isotropic and homogeneous, and the dielectric response of at least one of the material components needs to be negative. In practice, this introduces very significant problems with optical losses.

Here we demonstrate, with a numerically modeled super-resolution imaging experiment, a "Quantum Metamaterial" (QM) lens. It uses nanoscale quantum confinement to tailor the dielectric response of the individual metamaterials' components, as theoretically discussed in ref 15. It allows an extreme form of dichroism to be designed into them. This adds an extra element of design freedom because the dichroic effects (which result from the effects of quantum confinement on the electron transitions) can be tuned independently of the geometry-based "effective-medium" electromagnetic tuning of the metamaterial response function. In particular, we show how this new paradigm can be used to generate superresolution in a test QM structure without needing to incorporate any negative-response components. This latter structure exhibits a highly eccentric elliptical isofrequency dispersion characteristic that delivers λ/10 low-loss, super-resolution from a superlens that is significantly thicker (1.8 μm) than previously studied.

Previous super-resolution experiments[6] have used multi-periodic bilayers, to synthesize a hyperbolic[9,13] isofrequency dispersion characteristic (IDC), i.e., one with in-plane and out-of-plane dielectric responses that are opposite in sign. If we denote the thickness and permittivity of each of the bilayer components as ϵ_1, d_1 and ϵ_2, d_2, respectively, and assume that
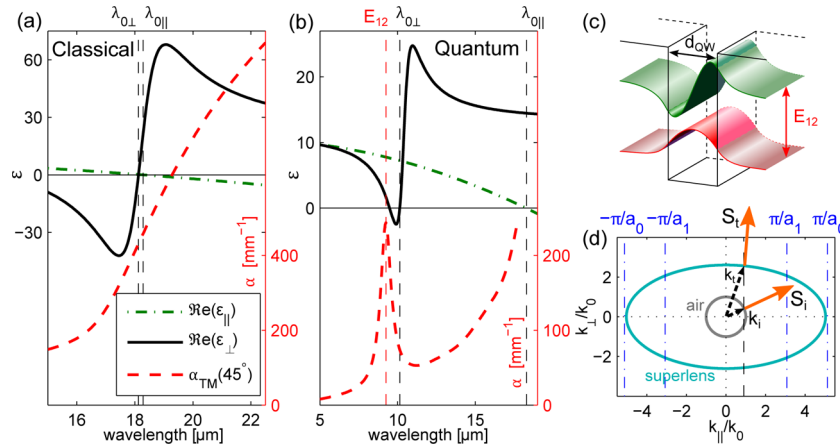
Figure 1. Optical responses of a metamaterial comprising an ideal dielectric ($\epsilon_{02} = 10.01$) and an equally thick ($d_1 = d_2 \ll \lambda$) $n = 4 \times 10^{18}$ cm^{-3} doped layer. The plots are of the real parts of the effective-medium permittivity for fields polarized in-plane ($\varepsilon_\parallel$, green dot-dash line) and out-of-plane ($\varepsilon_\perp$, black solid line) and loss factors (α, red dashed curve, calculated for light traveling at 45° to the layer). (a) "Classical" metamaterial, where the layer thicknesses are much shorter than the optical wavelength, but not small enough for quantum effects to come into play, and (b) the much thinner ($d_1 = d_2 = 8.1$ nm) layers of the "Quantum Metamaterial". $\lambda_{0\parallel}$ and $\lambda_{0\perp}$ (black dashed lines) are the wavelengths at which the dielectric functions change sign, and in the QM case they can be spectrally separated by the effects of quantum confinement in the nanostructure. (c) Schematic of the intersubband transition responsible for the optical resonance in the QM case; in the classical case the dispersive resonance arises from surface plasmon excitations at the layer interfaces. (d) The resulting QM elliptical iso-frequency dispersion curves (IDCs) and typical Poynting vectors for incident radiation, S_i, and as it is being transmitted through the QM, S_t. The vertical dashed lines correspond to the $k_\parallel$ values corresponding to the two sets of the dots ($a_0 = 1.2$ μm and $a_1 = 2$ μm dot diameters) highlighted in the experimental images of Figure 4.

both layers are much thinner than the optical wavelength in the slab, we have the averaging equations

$$\varepsilon_\perp = \frac{(d_1 + d_2)\epsilon_1\epsilon_2}{d_1\epsilon_2 + d_2\epsilon_1} \tag{1}$$

$$\varepsilon_\parallel = \frac{d_1}{(d_1 + d_2)}\epsilon_1 + \frac{d_2}{(d_1 + d_2)}\epsilon_2 \tag{2}$$

for the effective-medium responses of the multilayer to in-plane ($\varepsilon_\parallel$) and out-of-plane ($\varepsilon_\perp$) electric field components.

Typically, ϵ_1 comes from the Drude response of a metal or doped semiconductor, operated below its plasma frequency, ω_p ($\epsilon_1 < 0$),

$$\epsilon_1 = \epsilon_{01}\left(1 - \frac{\omega_p^2}{\omega^2 + i\omega/\tau}\right) \tag{3}$$

where ϵ_{01} is the background dielectric constant of layer 1 and ϵ_2 = $\epsilon_{02} > 0$ is the background dielectric constant of layer 2, assumed to be a near-ideal dielectric.

As previously pointed out by Salandrino and Engehta,[13] a judicious choice of the ratio d_1/d_2 can result in an "epsilon-near-zero" (ENZ) characteristic where, simultaneously, $\varepsilon_\perp < 0$ and $\varepsilon_\parallel > 0$ and also $|\varepsilon_\parallel| \ll |\varepsilon_\perp|$. In this case the IDCs become shallow hyperbolae that are flat over a wide range of $k_\parallel$ values. Since light propagates through the multilayer with a Poynting vector, S, that is normal to the IDC, this situation can result in light propagating through the multilayer in a near diffraction-less manner. In principle at least, this diffractionless propagation characteristic can extend out to large $k_\parallel$ values, so the light can traverse an arbitrary thickness of ENZ multilayer to generate a super-resolved image at its far side. In practice the utility of the effect is limited by the fact that the IDCs are not quite flat and that losses in the material component layers both dim the transmitted image to the point where it becomes unusable and blur it by absorbing the large $k_\parallel$

Fourier components that contain the super-resolution image information. Our QM superlens works through a similar, near-diffractionless, propagation effect as in the ENZ material, but it replaces the hyperbolic IDC with the highly eccentric elliptical IDC of Figure 1d, and it exploits quantum design techniques to reduce the loss.

The "quantum" aspect of the design is critical because it allows us to design the in- and out-of-plane dielectric responses in the QM independently. The importance of this can be seen in Figure 1a,b, where the in- and out-of-plane effective medium dielectric responses are plotted for a $d_1 = d_2$ semiconductor multilayer. In the "classical" case (Figure 1a), although d_1 and d_2 are both much smaller than the optical wavelength (as is the case in any metamaterial), they are both large compared with a typical electron wavelength, so the optical response of each component of the bilayer is isotropic. The consequence of this is that the wavelengths, $\lambda_{0\parallel}$ and $\lambda_{0\perp}$, where in- and out-of-plane metamaterial effective-medium responses, $\varepsilon_\parallel$ and $\varepsilon_\perp$, respectively, change sign, are the same to within a fraction of a percent (see the mathematical analysis in the Supporting Information). The superlens operates at a wavelength close to $\lambda_{0\perp}$; so in the "classical" case, this inevitably lies close to spectral region where $\varepsilon_\parallel$ is metallic and the losses are high.

In the QM example (Figure 1b), the bilayer component thicknesses are now shrunk to nanometer dimensions[16] so as to quantize the momenta of the electron states in the out-of-plane direction. The in-plane response, $\varepsilon_\parallel$, is still given by eq 2 and eq 3, but now the out-of-plane response, $\varepsilon_\perp$, originates in an independently tunable quantum mechanical intersubband transition (ISBT[17]), which gives the atomic-like absorption spectrum depicted in the red dashed curve of Figure 1b. The absorption spectrum is now a sharp peak, centered at the ISBT energy, E_{12} (see details in Supporting Information). This now allows $\lambda_{0\parallel}$ and $\lambda_{0\perp}$ to be designed to be widely separated. In the specific example of Figure 1, the QM effect shortens $\lambda_{0\perp}$ from ~18 μm to ~10 μm, and it opens up a spectral window where $\varepsilon_\perp$ and $\varepsilon_\parallel$ are, simultaneously, both positive and have widely
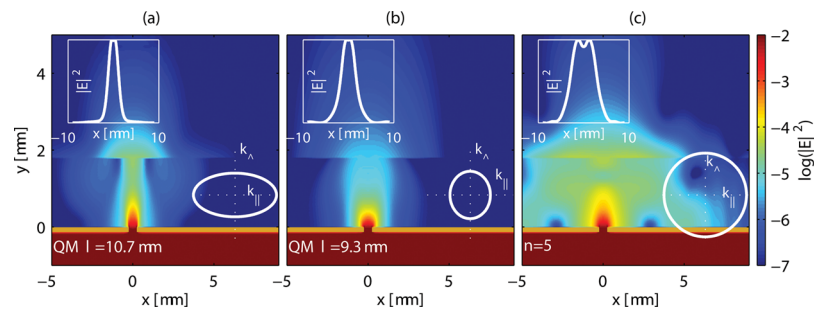
Figure 2. Modeled intensity distributions, from a single, ~$\lambda/20$, 500 nm diameter circular hole, centered at $x = y = 0$ and illuminated from below, as the beam propagates through three types of 1.8 μm thick imaging slab. (a) The QM slab of Figure 1b, operating at the $\lambda = 10.7$ μm resonance as in Figure 4b. (b) The same QM structure, operated off resonance ($\lambda = 9.3$ μm). (c) Hypothetical, isotropic $n = 5$ slab to check that the resolution enhancement is not solely due to the increased mean refractive index in the QM slab, but is due to the customized dielectric anisotropy resulting from the QM design (see also Figure S1 in the Supporting Information for E_z plots). Insets: superlens' dispersion curves, and lateral intensity plots at the top surface of the superlens, with full width at half-maximum values of 2.5, 3.6, and ~6 μm, for cases a, b, and c, respectively.
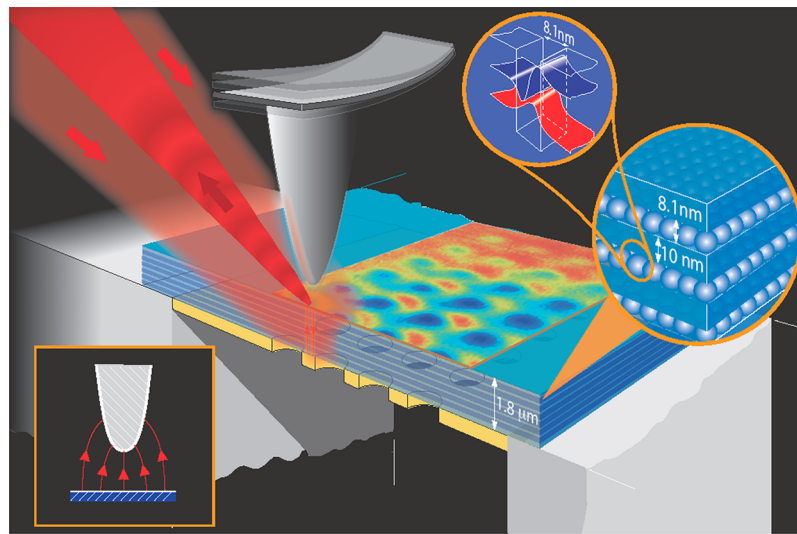

Figure 3. Schematic of the experimental arrangement. Infrared laser light illuminates a region surrounding the vertically oscillating probe of a scattering-scanning-nearfield-optical-microscope (s-SNOM). First the light travels down through the 1.8 μm thick "Quantum Metamaterial" superlens to illuminate the patterned metal mask below. The superlens then images the light reflected from this mask, and the intensity distribution at its upper surface is mapped out by rastering the tip across the sample and detecting the near-field light it scatters using a phase-sensitive interferometric scheme.[22]

different values. This gives the highly elliptical IDCs of Figure 1d that we can use to make super-resolution devices

The fact that the QM approach allows us to work in a regime where the dielectric responses are all positive means that the losses are some 10× lower than in previously reported superresolution schemes. This can be seen by comparing the red-dashed loss curves in Figure 1a,b, the loss factors at the operating wavelength, $\lambda \approx \lambda_{0\perp}$ in the QM case (~40 mm^{-1}), are almost 10× lower than in the "classical" case (~400 mm^{-1}). This gives a dramatic improvement in the loss figure of merit, defined as FOM $\equiv$ Re$[K_{TM}]$/Im$[K_{TM}]$, where K_{TM} is the wave vector of the transverse magnetic polarization.[8] For our QM, the FOM $\approx$ 80, compared with FOM $\approx 10^{-2}$ to ~1 reported for metal−dielectric systems,[18] FOM $\approx$ 4 for hyperlenses working at the ~1610 cm^{-1} optical phonon resonance of hexagonal boron nitride,[19−21] and FOM $\approx$ 10 for "classical" doped semiconductor systems.[8]

To evaluate the imaging potential of such a QM superlens, a standard finite-difference-time-domain (FDTD) method was used to simulate an imaging experiment (Figure 2) consisting of a 500 nm (~$\lambda/20$) diameter circular hole in a gold mask. It

was illuminated, with plane wave illumination at normal incidence from below, and imaged with a 1.8 μm thick QM superlens, at wavelengths close to the $\lambda \approx \lambda_{0\perp}$ operating point.

Two simulations were performed. The first modeled the QM itself, using the approach of ref 15, seeded with the experimentally measured (see Supporting Information) carrier densities and scattering rates, to compute the effective-medium metamaterial response tensor. The second was a control simulation, in which the QM superlens slab was replaced with an equally thick slab of a hypothetical isotropic $n = 5$ lossless dielectric. This was to separate the effects of the ellipticity in the QM from the possibility of simple near field concentration effects that might arise simply due to the heightened overall refractive index at resonance.

Modeling the imaging of the QM superlens at its $\lambda = 10.7$ μm optimum resonance (Figure 2a) shows a pronounced "beaming" characteristic, i.e., the near-diffractionless propagation characteristic previously seen in ENZ hyperlenses.[13] The modeled radiation patch has a full width at half-maximum (fwhm) of 2.5 μm, i.e., the QM superlens can successfully reproduce lateral image detail at the top surface at levels
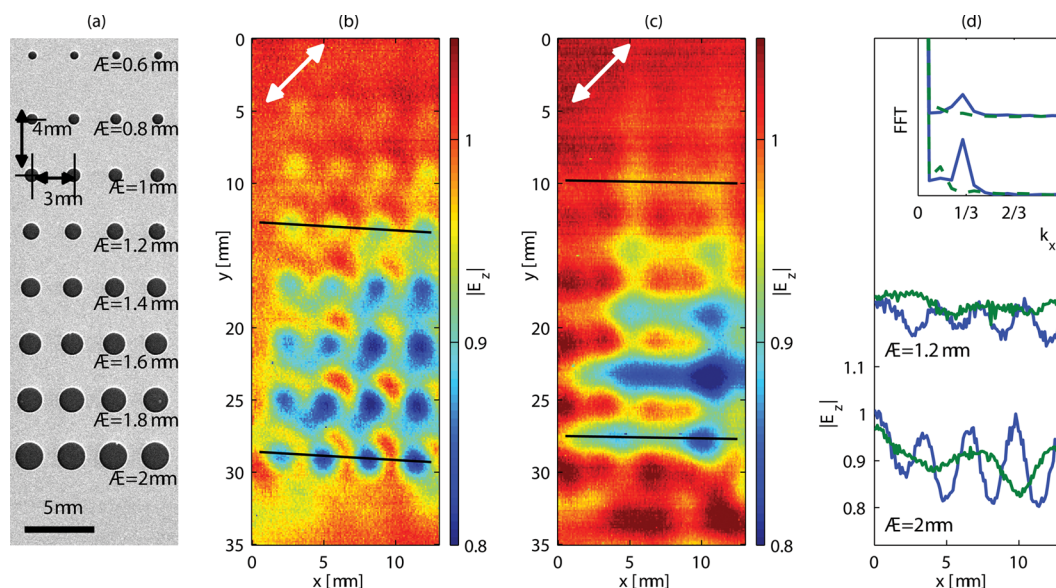
Figure 4. (a) Electron microscope image of the metal mask taken from beneath the sample. (b) s-SNOM image of the mask, taken in reflection mode (Figure 3), through the "Quantum Metamaterial" superlens with $\lambda = 10.7\ \mu m$ wavelength light. (c) Same as that in panel b but with the wavelength shortened to $\lambda = 9.3\ \mu m$. (d) Intensity line scans and their spatial Fourier transforms taken along the images of the centers of the 1.2 μm (upper trace) and the 2 μm diameter dots, as shown by the black tracking lines in panels b and c. The holes in panel b are resolved down to a diameter of $\sim 0.8\ \mu m$. The blue traces correspond to the $\lambda = 10.7\ \mu m$ panel b, i.e., when the QM superlens is operating at its optimum resonance and the green traces correspond to panel c, i.e., where the wavelength has been shortened away from this resonance, by $\sim 14\%$, to $\lambda = 9.3\ \mu m$. The double headed arrows in panels b and c indicate the polarization of the incident radiation.

dramatically below the $\sim 10\ \mu m$ diffraction limit. Moreover, detuning the wavelength only slightly ($\sim 14\%$) away from the optimum value (Figure 2b) is enough to reduce the image sharpness by a factor of ~ 1.44, and the intensity by roughly a decade. Taken together these effects imply that the electronic ISBT resonance designed in the QM material is the cause of the super-resolution. This level of image detail is completely unmatched in the $n = 5$ control sample (Figure 2c), where the image is blurred into a much larger, essentially diffraction-limited spot, $\sim 6\ \mu m$ across, at the top surface of the slab, again confirming that the resolution enhancement really does come from the designed-in QM anisotropy.

As a practical demonstration, a 1.8 μm thick QM slab was fabricated, using standard molecular beam epitaxy techniques, from a semiconductor "multiple quantum well" (MQW) stack (see Supporting Information) comprising 100 repeats of a bilayer consisting of 10 nm of undoped $Al_{0.3}Ga_{0.7}As$ and 8.1 nm $n = 4.1 \times 10^{18}\ cm^{-3}$ doped GaAs. Separate measurements indicated the presence of an ISBT that gave a strong absorption peak centered at $E_{12} = 129.7$ meV and half-width at half-maximum $\Gamma \approx 8$ meV. An optimum wavelength of $\lambda \approx 10.7\ \mu m$ for the super-resolution effect was calculated for this structure using the theoretical approach described in ref 15. The QM slab was removed from its growth substrate, inverted, and mounted on a silicon wafer holder with a ~ 1 mm diameter through-hole for the imaging experiments. Its lower surface was coated with a 60 nm thick gold layer, which was patterned with a mask array of variously sized circular holes. These holes were then imaged through the QM superlens (Figure 3) using a near-field "scattering-scanning-near-field-optical-microscope" (s-SNOM).

In the experiment, practical considerations dictated that the mid-IR imaging radiation (from a CO_2 laser) had to impinge on the QM slab from above, at $\sim 60°$ to its surface normal (Figure 3). After the incident light passes through the QM slab to illuminate the mask below, an image of the mask, in reflection,

propagates back up through the QM slab, in a near diffractionless manner, to create a super-resolved image on its top surface.[10] This super-resolved image is then recorded by probing its near field image components by detecting the light scattered by the sharp, oscillating s-SNOM probe tip[22] (Figure 3).

The resulting images (Figure 4) show that, contrary to the usual tendencies of diffraction, the image detail sharpens significantly as the wavelength is lengthened (from $\lambda = 9.3\ \mu m$ to $\lambda = 10.7\ \mu m$). At the longer wavelength the QM superlens gives an extremely high quality image; the 0.8 μm diameter dots are resolved, corresponding to a deep subwavelength resolution, better than $\sim \lambda/10$ in this instance. The dramatic improvement in resolution, caused by such a small ($\sim 14\%$) change in wavelength, is consistent with the effect originating from the sharply resonant ISBT feature in the QM optical response with an elliptical IDC of Figure 1d. As a quantitative measure of the change in image sharpness, a series of line scans were taken along the rows of 1.2 and 2 μm diameter dots. In both cases the intensity modulation practically vanishes when the operating wavelength is shifted from $\lambda = 10.7\ \mu m$ to $\lambda = 9.3\ \mu m$. As a quantitative measure, the first harmonic peaks in the spatial Fourier transforms of the images of the periodic hole arrays (Figure 4d, upper traces) were computed. They were found to drop below the noise floor in the $\lambda = 9.3\ \mu m$ image. This implied an image sharpening of a factor of >25 for the 2 μm holes and >6.2 for the 1.2 μm holes as the wavelength is tuned to the QM resonance from a wavelength that is only $\sim 14\%$ away from it.

Figure 1c shows how the in-plane spatial frequency components (π/a_n), required to resolve the different hole diameters (a_n), relate to the modeled IDC for the QM superlens. This shows how the high degree of eccentricity that the QM approach has allowed us to engineer into the IDC gives the superlens slab the ability to image holes down to, in

this case, $a_0 \approx 1 \ \mu$m. It does this via a near-diffractionless propagation effect that is analogous to that previously reported for ENZ hyperlenses.[13]

Finally, we note that these highly eccentric elliptical QM superlens materials also lend themselves to the fabrication of a variety of 3D structures[6,7,13,14] that can, in principle, extend the near field image information out to a far field distribution that could be interrogated with conventional diffraction-limited optical systems. The lowered losses that QM devices offer compared with ENZ materials may ultimately offset the additional effort required to fabricate them.

■ ASSOCIATED CONTENT

Ⓢ Supporting Information

The Supporting Information is available free of charge on the ACS Publications website at DOI: 10.1021/acs.nanolett.5b04300.

> Mathematical analysis of the loss mechanisms in "classical" metamaterials; technical details and materials parameters used for the numerical modeling; details of the QM superlens fabrication process; technical details of the s-SNOM imaging experiment (PDF)

■ AUTHOR INFORMATION

Corresponding Author
*E-mail: chris.phillips@imperial.ac.uk.

Notes
The authors declare the following competing financial interest(s): R.H. is co-founder of Neaspec GmbH, a company producing scattering-type scanning near-field optical microscope systems such as the one used in this study. All other authors declare no competing financial interest.

■ REFERENCES

(1) Pendry, J. Negative Refraction Makes a Perfect Lens. *Phys. Rev. Lett.* **2000**, *85*, 3966.

(2) Schurig, D.; Mock, J. J.; Justice, B. J.; Cummer, S. A.; Pendry, J. B.; Starr, A. F.; Smith, D. R. Metamaterial Electromagnetic Cloak at Microwave Frequencies. *Science* **2006**, *314*, 977.

(3) Fleury, R.; Alu, A. Manipulation of electron flow using near-zero index semiconductor metamaterial. *Phys. Rev. B: Condens. Matter Mater. Phys.* **2014**, *90*, 035138.

(4) Valentine, J.; Li, J.; Zentgraf, T.; Bartal, G.; Zhang, X. An optical cloak made of dielectrics. *Nat. Mater.* **2009**, *8*, 568.

(5) Fang, N.; Lee, H.; Sun, C.; Zhang, X. Sub−Diffraction-Limited Optical Imaging with a Silver Superlens. *Science* **2005**, *308*, 534.

(6) Liu, Z.; Lee, H.; Y Xiong, Y.; C Sun, C.; Zhang, X. Far-Field Optical Hyperlens Magnifying Sub-Diffraction-Limited Objects. *Science* **2007**, *315*, 1686.

(7) Dong, J.; Liu, J.; Zhao, X.; Liu, P.; Liu, J.; Kang, G.; Xie, J.; Wang, Y. A Super Lens System for Demagnification Imaging Beyond the Diffraction Limit. *Plasmonics* **2013**, *8*, 1543.

(8) Hoffman, A. J.; Alekseyev, L.; Howard, S. S.; Franz, K. J.; Wasserman, D.; Podolskiy, V. A.; Narimanov, E. E.; Sivco, D. L.; Gmachl, C. Negative refraction in semiconductor metamaterials. *Nat. Mater.* **2007**, *6*, 946.

(9) Poddubny, A.; Iorsh, I.; Belov, P.; Kivshar, Y. Hyperbolic metamaterials. *Nat. Photonics* **2013**, *7*, 948.

(10) Taubner, T.; Korobkin, D.; Urzhumov, Y.; Shvets, G.; Hillenbrand, R. Near-Field Microscopy Through a SiC Superlens. *Science* **2006**, *313*, 1595.

(11) Choe, J.-H.; Choi, M.; Lee, W. J.; Kang, B.; Kim, J.; Seo, M.-K.; Min, B.; Kim, S.; Choi, C.-G.; et al. Subwavelength imaging in the visible range using a metal coated carbon nanotube forest. *Nanoscale* **2014**, *6*, 5967.

(12) Li, P.; Wang, T.; Bőckmann, H.; Taubner, T. Graphene-Enhanced Infrared Near-Field Microscopy. *Nano Lett.* **2014**, *14*, 4400.

(13) Salandrino, A.; Engheta, N. Far-field subdiffraction optical microscopy using metamaterial crystals: Theory and simulations. *Phys. Rev. B: Condens. Matter Mater. Phys.* **2006**, *74*, 075103.

(14) Lu, D.; Liu, Z. Hyperlenses and metalenses for far-field super-resolution imaging. *Nat. Commun.* **2012**, *3*, 1205.

(15) Bak, A. O.; Giannini, V.; Maier, S. A.; Phillips, C. C. Super-resolution with a positive epsilon multi-quantum-well super-lens. *Appl. Phys. Lett.* **2013**, *103*, 261110.

(16) Plumridge, J.; Clarke, E.; Murray, R.; Phillips, C. C. Ultra-Strong Coupling Effects with Quantum Metamaterials. *Solid State Commun.* **2008**, *146*, 406.

(17) Zaluzny, M.; Nalewajko, C. Coupling of infrared radiation to intersubband transitions in multiple quantum wells: The effective-medium approach. *Phys. Rev. B: Condens. Matter Mater. Phys.* **1999**, *59*, 13043.

(18) Saha, B.; Naik, G. V.; Saber, S.; Akatay, C.; Stach, E. A.; Shalaev, V. M.; Boltasseva, A.; Sands, T. D. TiN/(Al,Sc)N metal/dielectric superlattices as hyperbolic metamaterials in the visible spectral range. *Phys. Rev. B: Condens. Matter Mater. Phys.* **2014**, *90*, 125420.

(19) Dai, S.; et al. Subdiffractional focusing and guiding of polaritonic rays in a natural hyperbolic material. *Nat. Commun.* **2015**, *6*, 6963.

(20) Li, P. Hyperbolic phonon-polaritons in boron nitride for near-field optical imaging and focusing. *Nat. Commun.* **2015**, *6*, 7507.

(21) Dai, S.; et al. Tunable Phonon Polaritons in Atomically Thin van der Waals Crystals of Boron Nitride. *Science* **2014**, *343*, 1125.

(22) Keilmann, F.; Hillenbrand, R. Near-field microscopy by elastic light scattering from a tip. *Philos. Trans. R. Soc., A* **2004**, *362*, 787.

■ NOTE ADDED AFTER ASAP PUBLICATION

This paper was published on the Web on February 10, 2016, with errors in Figure 1. The corrected version was reposted on March 9, 2016.